

Active Learning for Planet Habitability Classification under Extreme Class Imbalance

R. I. EL-KHOLY ¹ AND Z. M. HAYMAN ¹

¹*Department of Astronomy, Space Science, and Meteorology
Faculty of Science, Cairo University
1 Gamaa Street, Giza 12613, Egypt*

(Received March 2, 2026; Revised March 2, 2026; Accepted March 2, 2026)

Submitted to PASP

ABSTRACT

The increasing size and heterogeneity of exoplanet catalogs have made systematic habitability assessment challenging, particularly given the extreme scarcity of potentially habitable planets and the evolving nature of their labels. In this study, we explore the use of pool-based active learning to improve the efficiency of habitability classification under realistic observational constraints. We construct a unified dataset from the Habitable World Catalog and the NASA Exoplanet Archive and formulate habitability assessment as a binary classification problem. A supervised baseline based on gradient-boosted decision trees is established and optimized for recall in order to prioritize the identification of rare potentially habitable planets. This model is then embedded within an active learning framework, where uncertainty-based margin sampling is compared against random querying across multiple runs and labeling budgets. We find that active learning substantially reduces the number of labeled instances required to approach supervised performance, demonstrating clear gains in label efficiency. To connect these results to a practical astronomical use case, we aggregate predictions from independently trained active-learning models into an ensemble and use the resulting mean probabilities and uncertainties to rank planets originally labeled as non-habitable. This procedure identifies a single robust candidate for further study, illustrating how active learning can support conservative, uncertainty-aware prioritization of follow-up targets rather than speculative reclassification. Our results indicate that active learning provides a principled framework for guiding habitability studies in data regimes characterized by label imbalance, incomplete information, and limited observational resources.

Keywords: Exoplanet catalogs (488) — Exoplanets (498) — Habitable planets (695) — Algorithms (1883) — Astrostatistics techniques (1886) — Classification (1907)

1. INTRODUCTION

The increasing scale and complexity of modern astronomical surveys have intensified the need for machine learning (ML) methods capable of extracting reliable scientific insights from large, heterogeneous datasets. In many astronomical applications, the primary bottleneck is not data availability but the scarcity of reliable labels, which often require costly follow-up observations or expert analysis (J. W. Richards et al. 2011). Active learning (AL) addresses this challenge by enabling mod-

els to iteratively select the most informative unlabeled instances for annotation, thereby improving predictive performance while minimizing labeling effort (E. E. O. Ishida et al. 2018; P. Škoda et al. 2020).

AL differs fundamentally from conventional supervised learning by replacing static or random training set construction with a sequential querying process. At each iteration, the learner identifies data points whose labels are expected to yield the greatest improvement to the model, querying an oracle for their true labels. This approach has proven effective in settings where labeled data are limited, expensive, or unevenly distributed, making it particularly relevant for many astronomical problems (T. Solorio et al. 2005; J. W. Richards et al. 2011; D. Masters et al. 2015; B. Hoyle et al. 2016).

In astronomy, AL has been successfully applied to a range of tasks, including variable star classification (J. W. Richards et al. 2011), supernova photometric classification (E. E. O. Ishida et al. 2018, 2021; N. Kenamer et al. 2020; M. Leoni et al. 2022), galaxy morphology classification (M. Walmsley et al. 2019), stellar parameters inference (R. El-Kholy & Z. Hayman 2025), and anomaly detection in large survey datasets (E. E. O. Ishida et al. 2021; M. Lochner & B. Bassett 2021). These studies demonstrate that AL can significantly improve model performance or reduce labeling requirements when compared to random sampling strategies, particularly in scenarios characterized by high data volume and limited labeling resources.

However, prior work (H. Zhang et al. 2018; H. Yu et al. 2019; Y. Quan et al. 2021) has also highlighted several challenges associated with applying AL in astronomical contexts. A recurring issue is severe class imbalance, where scientifically interesting objects constitute a small fraction of the overall dataset. Under such conditions, common uncertainty-based querying strategies may perform suboptimally, motivating careful evaluation of AL behavior in imbalanced regimes.

Despite the breadth of AL applications in astronomy, its use in the context of exoplanet habitability assessment remains notably unexplored. Existing ML studies on planet habitability focus primarily on supervised classification (S. Saha et al. 2018, 2020; S. Basak et al. 2021), regression-based habitability indices (D. Schulze-Makuch et al. 2011; J. M. Rodríguez-Mozos & A. Moya 2017; Y. Patel 2024; R. Dhama et al. 2025), or architectural comparisons (R. Barnes et al. 2015), without considering AL as a means of addressing label scarcity or prioritizing follow-up observations. This omission is striking given they are inherently uncertain, sparse, and costly to validate, and that exoplanet datasets are typically highly imbalanced.

This work addresses this gap by investigating the application of AL to planet habitability classification. Building on established AL methodologies developed in astronomical and ML contexts, we evaluate whether uncertainty-driven instance selection can improve classification performance relative to random sampling under realistic data constraints. We further examine the implications of AL for prioritizing candidate planets for further study. The methodology and experimental design are described in Section 2, with results presented in Section 3 and their implications discussed in Section 4. We give our final conclusions in Section 5. All data and

source code used in this study are made available in a public GitHub repository².

2. DATA AND METHODS

2.1. Dataset and feature selection

In this work, two publicly available data sources were used. The first is the Habitable Worlds Catalog (HWC) (PHL @ UPR Arcibo 2025), which lists 70 potentially habitable worlds out of over 5000 known exoplanets. They are further divided into a conservative and optimistic sample. The conservative subset comprises planets with radii not exceeding 1.6 Earth radii or masses below 3 Earth masses, which are more likely to be rocky in composition. The optimistic subset extends to larger planets, potentially encompassing super-Earths, ocean worlds, or mini-Neptunes, which are correspondingly less likely to be rocky or to sustain surface liquid water. We used a version of the full catalog downloaded on 22 October 2025.

The HWC primarily draws its exoplanet parameters from the Planetary Systems Composite Parameters (PSCCompPars) table of the NASA Exoplanet Archive³, which is the second source we used (J. L. Christiansen et al. 2025), also downloaded on 22 October 2025. However, the HWC is supplemented by additions and corrections from other literature sources. While this approach yields a more comprehensive collection of planetary properties, it also introduces potential inconsistencies arising from the aggregation of independent measurements. Consequently, the HWC is best regarded as a reference framework to guide further investigation rather than a definitive classification of planetary habitability. Because individual references do not necessarily report a complete set of stellar and planetary properties, the PSCCompPars table itself consolidates measurements from multiple references into a single row per confirmed planet. This aims to maximize parameter completeness by selecting preferred values across sources, yielding a more filled-in representation of planetary and stellar properties. However, this increased completeness comes at the expense of strict self-consistency, as the reported parameters may originate from different studies employing distinct assumptions or methodologies. Accordingly, the PSCCompPars table is well suited for statistical and ML applications that require broad feature coverage, but its contents should be interpreted with appropriate caution.

² <https://github.com/rehamelkholy/ExoplanetAL>

³ <https://exoplanetarchive.ipac.caltech.edu/index.html>

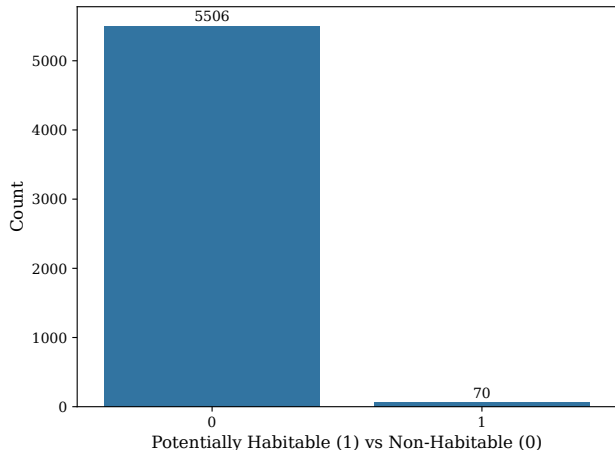


Figure 1. Distribution of habitability labels after cross-matching the Habitable Worlds Catalog with confirmed exoplanets from the NASA Exoplanet Archive. The dataset is highly imbalanced, with potentially habitable planets representing a small fraction of the confirmed population.

The downloaded version of the HWC contained 5599 exoplanets, while the PSCompPars table contained 6028 exoplanets. The two datasets were merged by cross-matching the planetary names. The resulting merged dataset contained 5576 exoplanet, including the 70 potentially habitable planets, as shown in Figure 1.

The feature selection process was designed to construct a physically meaningful and internally consistent representation of planetary, stellar, and system properties, while making maximal use of the information available across the two source catalogs. Following the cross-matching of the HWC and the PSCompPars table, all quantitative parameters from both sources were initially retained in a merged dataset to allow explicit evaluation of overlap and redundancy.

Because the two catalogs report many of the same physical quantities—such as orbital parameters, planetary size and mass estimates, and stellar properties—the merged dataset contains multiple column pairs describing identical or closely related attributes. As a first step in resolving this redundancy, the degree of agreement between corresponding columns from the two sources was assessed using pairwise correlation analysis. This analysis confirmed that overlapping parameters from HWC and PSCompPars are strongly correlated, indicating that they encode the same underlying physical information rather than independent measurements.

After establishing this equivalence, redundancy was resolved by comparing the completeness of each overlapping column pair. For each physical quantity represented in both catalogs, the column exhibiting superior overall completeness was selected as the primary repre-

sentation and retained for subsequent analysis. Following this selection, the redundant column from the other source was used exclusively to supplement missing values in the retained column wherever possible. This ensured that each physical quantity is represented by a single unified column in the final dataset. Once supplementation was complete, the redundant columns were removed.

The resulting feature set was then examined through exploratory analysis conducted entirely on this final, unified set of features. Pairwise correlations among retained features were inspected to characterize dependencies arising from known physical relationships. The resulting visualization is shown in Figure 2. It reveals several physically expected dependencies. Strong positive correlations are observed among stellar properties, particularly between stellar radius and stellar luminosity, reflecting underlying stellar structure relations. Planetary radius and planetary mass also show a moderate positive correlation, consistent with known mass-radius trends for exoplanets. Incident stellar flux and planetary equilibrium temperature are moderately correlated, as expected from their shared dependence on stellar luminosity and orbital separation. A notable moderate negative correlation is observed between Earth Similarity Index (ESI) (D. Schulze-Makuch et al. 2011) and planetary radius, indicating that larger planets tend to score lower on Earth-likeness metrics. Importantly, no pair of retained features exhibits near-perfect correlation outside of these physically motivated relationships, suggesting that the final feature set does not suffer from severe multicollinearity. This supports the suitability of the selected variables for subsequent ML and AL analyses.

The structure of missing values in the final dataset is summarized in Figure 3 using an UpSet (A. Lex et al. 2014) representation. The plot reveals that missingness is not uniformly distributed across features, but instead exhibits clear patterns. Orbital eccentricity accounts for the largest share of missing values, frequently occurring as the sole missing parameter in otherwise complete records. In contrast, stellar luminosity, stellar radius, incident stellar flux, and planetary mass, radius, and density show comparatively low missingness. These structured missingness patterns indicate that absent values are primarily driven by observational and derivational limitations rather than random omission, motivating a targeted treatment of missing data in subsequent preprocessing steps (Section 2.3).

Figure 4 highlights the degree to which potentially habitable and non-habitable planets overlap in marginal feature space, emphasizing the intrinsic difficulty of

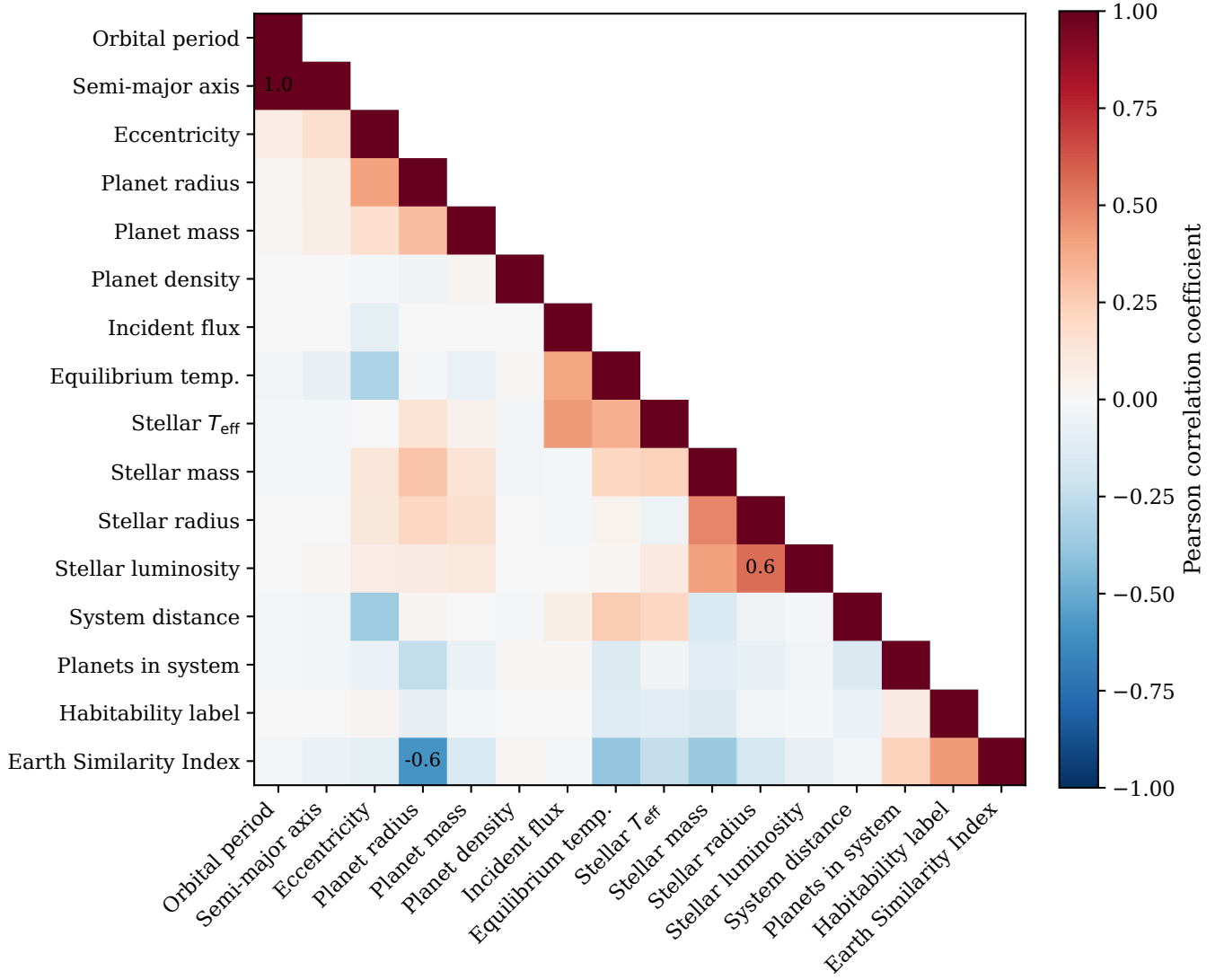


Figure 2. Lower-triangular Pearson correlation matrix of the final feature set used in this study. Each cell shows the Pearson correlation coefficient between a pair of planetary or stellar properties, with the color scale ranging from -1 (strong negative correlation) to $+1$ (strong positive correlation). The diagonal elements represent self-correlations. To improve readability, only moderate to strong correlations ($|r| \geq 0.5$) are annotated.

habitability classification based on any single parameter. While potentially habitable planets tend to cluster toward smaller radii and lower masses, the distributions remain broad and partially overlapping, reflecting both observational uncertainties and the inclusive definition of habitability adopted by the HWC. Incident stellar flux and equilibrium temperature exhibit clearer class separation when viewed on logarithmic scales, with potentially habitable planets concentrated near Earth-like fluxes and moderate equilibrium temperatures, whereas non-habitable planets span a much wider dynamic range. However, even in these parameters, no sharp decision boundary exists. Orbital eccentricity shows strong skewness toward low values in

both classes, with potentially habitable planets slightly more concentrated at near-circular orbits, consistent with expectations for long-term climate stability. The ESI provides the most visually distinct separation, by construction aggregating multiple planetary properties into a single heuristic score, yet still exhibits overlap between classes. Overall, these class-conditional distributions demonstrate that habitability cannot be reliably inferred from univariate thresholds alone. Instead, the substantial overlap across most features motivates the use of multivariate ML models and, in particular AL strategies capable of efficiently identifying informative regions of parameter space where class distinctions are most ambiguous. Together, the final features provide a

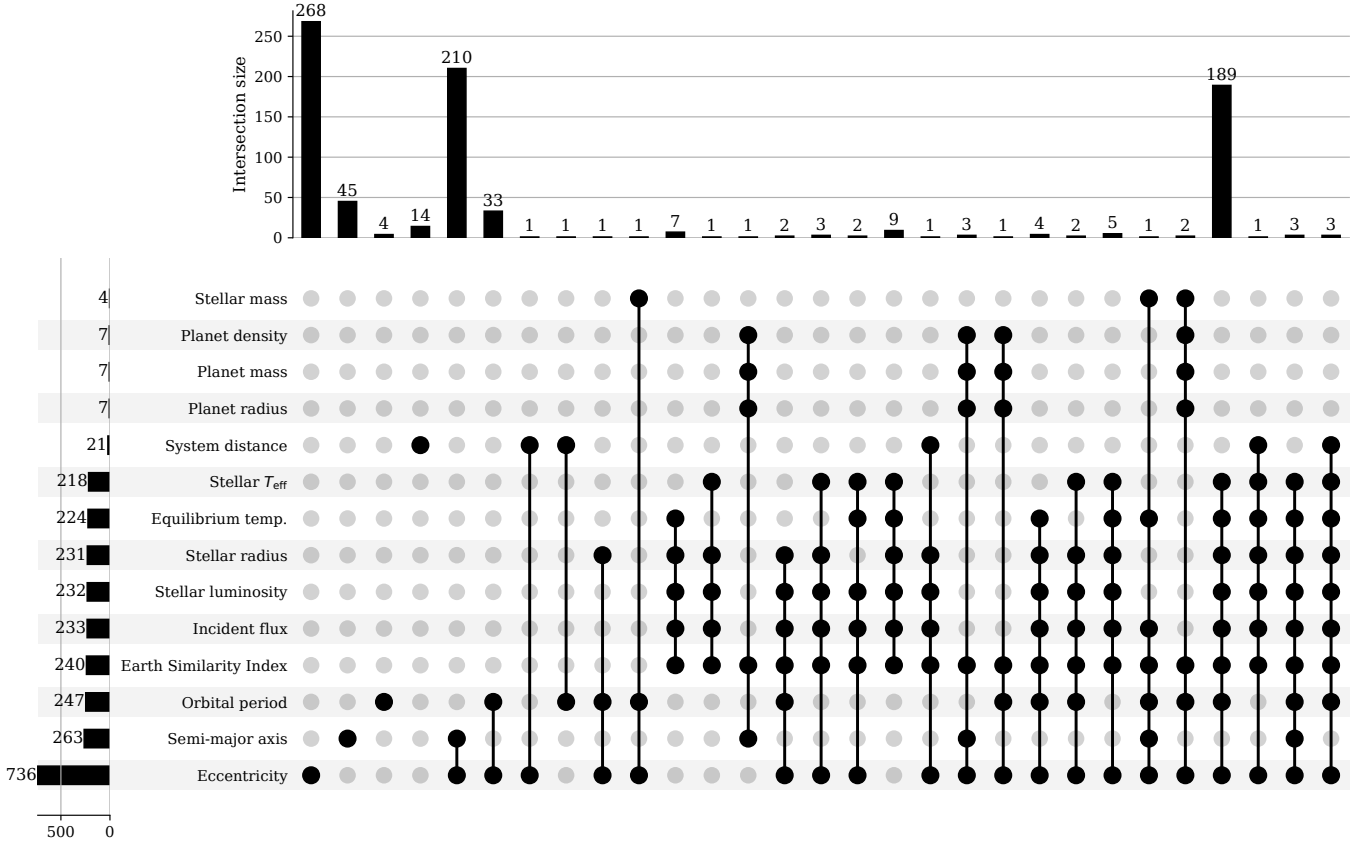


Figure 3. UpSet plot showing missing-value patterns across the final feature set. The horizontal bars on the left indicate the total number of missing values for each feature. Each column in the central matrix represents a specific combination of features that are simultaneously missing, marked by filled black circles connected by vertical lines. The vertical bars above the matrix show the number of data instances exhibiting each missingness pattern (intersection size). For example, the tallest bar on the far left corresponds to instances where only orbital eccentricity is missing, while all other features are present. In contrast, columns with multiple connected black circles indicate instances where several stellar and planetary properties are missing together.

compact yet physically interpretable description of each planetary system, balancing completeness and redundancy while preserving all dimensions relevant to habitability assessment.

2.2. Problem formulation

We formulate the task as a binary classification problem, where each confirmed exoplanet is assigned a label indicating whether it is potentially habitable or non-habitable based on current catalog assessments. Given a feature vector containing stellar, planetary, and system-level properties for a planet, the objective is to learn a classifier that maps the vector onto a binary output indicating whether the planet is classified as potentially habitable or non-habitable. This formulation reflects a practical observational setting in which habitability is treated as a prioritization signal rather than a definitive physical state. The classifier is therefore designed to

identify planets that merit further study under limited observational resources, rather than to determine true biological habitability.

Positive labels are derived from the HWC, which identifies planets that orbit within the stellar habitable zone and satisfy broad constraints on planetary size and mass, aiming to be inclusive while acknowledging substantial astrophysical uncertainties (PHL @ UPR Arcibo 2025). As mentioned in Section 2.1, the catalog subdivides potentially habitable planets into conservative and optimistic samples. In this study, both samples are labeled as potentially habitable. This choice reflects the study’s emphasis on accelerating candidate discovery rather than enforcing strict geophysical definitions. Treating the two samples jointly increased the number of positive instances and aligns with the goal of iden-

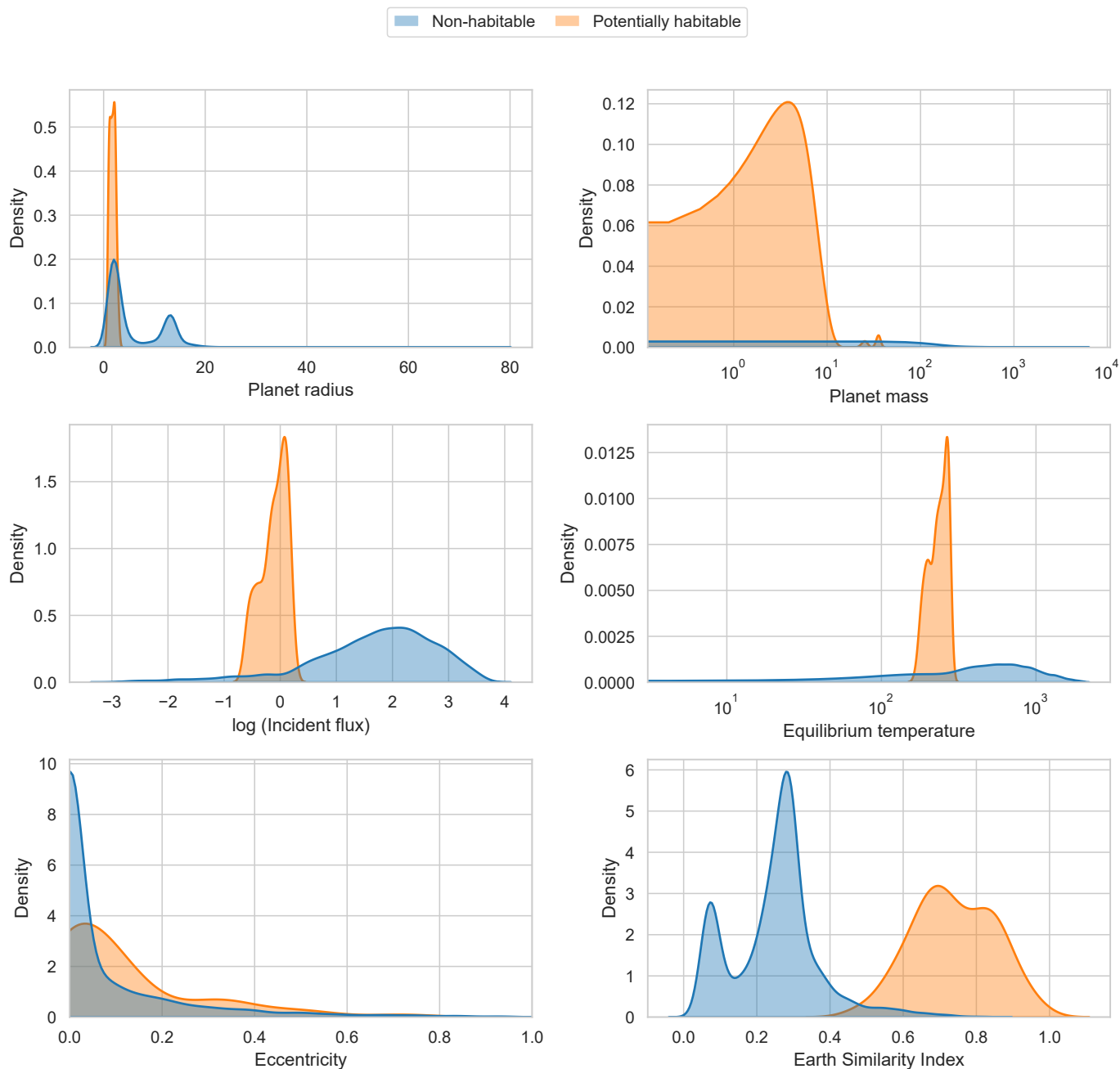


Figure 4. Class-conditional distributions of selected planetary and stellar parameters in the final dataset. Kernel density estimates are shown for planet radius, orbital eccentricity, and ESI; and in log scale for planet mass, incident stellar flux, and equilibrium temperature. The figure illustrates the substantial overlap between the two classes across most individual parameters, as well as systematic shifts in location and spread for several features, motivating the need for multivariate classification.

tifying planets worthy of follow-up observations under uncertainty.

Importantly, these labels should not be interpreted as ground truth indicators of actual habitability. As emphasized in the HWC documentation (PHL @ UPR [Arecibo 2025](#)), the criteria used to define habitability rely on simplified models (e.g., [D. Schulze-Makuch et al. \(2011\)](#); [R. K. Kopparapu et al. \(2014\)](#)), in-

complete measurements, and assumptions about atmospheric composition and planetary structure. Consequently, some positively-labeled planets may ultimately prove uninhabitable, while others currently labeled as non-inhabitable could later be revised. The labels therefore represent heuristic, literature-based assessments rather than definitive physical classifications. This inherent uncertainty motivates the use of ML models and

AL strategies that can operate effectively under label noise, class imbalance, and evolving understanding.

2.3. Preprocessing and missing-data handling

The merged dataset resulting from the feature selection stage (Section 2.1) required several preprocessing steps to address missing values and physical consistency prior to model training and AL. These steps were designed to minimize information loss while preserving plausibility and avoiding the introduction of bias into the habitability labels.

As a first step, we attempted to reduce missingness using deterministic physical relationships between planetary and stellar parameters wherever possible. This approach was preferred over statistical imputation when reliable formulae could be applied, as it preserves known astrophysical constraints. Only two such derivations were possible. For planets with a known orbital period and host stellar mass, missing values of the orbital semi-major axis were computed using Kepler’s third law,

$$a = \left(\frac{GM_\star P^2}{4\pi^2} \right)^{1/3}, \quad (1)$$

where a is the semi-major axis, P is the orbital period, M_\star is the stellar mass, and G is the gravitational constant. Planetary mass was neglected relative to the stellar mass, consistent with standard practice for exoplanetary systems. This relation allowed the recovery of 259 additional semi-major axis values, substantially reducing missingness in this parameter. For stellar systems with known stellar luminosity and effective temperature but missing stellar radius, the radius was derived using the Stefan-Boltzmann relation,

$$L_\star = 4\pi R_\star^2 \sigma T_{\text{eff}}^4, \quad (2)$$

which can be rearranged as

$$R_\star = \left(\frac{L_\star}{4\pi\sigma T_{\text{eff}}^4} \right)^{1/2}, \quad (3)$$

where L_\star , R_\star , and T_{eff} are stellar luminosity, radius, and effective temperature, respectively, and σ is the Stefan-Boltzmann constant. This relation resulted in one additional valid stellar radius value. After applying these relations, all derived values were validated against physical bounds.

Following physics-based completion, missing values were reassessed for both the full dataset and the subset of potentially habitable planets. Among the 70 planets labeled as potentially habitable, missing values were found only in orbital eccentricity (10 entries). All other features were complete for this class. Across the full

dataset, the remaining missing values were confined to a small number of parameters, including planetary density, incident flux, equilibrium temperature, stellar radius, stellar luminosity, and a small number of semi-major axis entries. Given the large size of the non-habitable class, rows with missing values in these features were removed, while rows missing only eccentricity were retained for imputation. This filtering resulted in a dataset of 5281 planets, preserving all potentially habitable instances while ensuring completeness for the remaining features.

Before imputation, all features were subjected to sanity checks to identify invalid or extreme values. These included enforcing non-negativity for quantities such as mass, radius, flux, and semi-major axis; and constraining orbital eccentricity to the physical range $[0, 1]$. No systematic anomalies were found beyond those already addressed through row removal or subsequent imputation.

Orbital eccentricity was imputed using a supervised regression approach trained on planets with complete feature vectors. From the 4803 planets with observed eccentricity, the data were split into an 80% training set and a 20% test set. A standard scaler was fitted on the training data and applied consistently to the test set and the rows requiring imputation. Two regressors were evaluated: a random forest regressor and a gradient boosting regressor. Model selection was based on mean absolute error (MAE) computed on the held-out test set. Gradient boosting achieved the lowest error and was therefore selected for imputation. To quantify uncertainty, seven imputation iterations were performed using bootstrap resampling of the training set while keeping hyperparameters fixed. For each missing entry, the final imputed value was computed as the mean of the seven predictions, and uncertainty was estimated as their standard deviation. All imputed values were clipped to the physical interval $[0, 1]$, and additionally constrained to lie within $[\min_{\text{neighbor}} - 3\sigma, \max_{\text{neighbor}} + 3\sigma]$, where neighboring values were defined in feature space.

Figure 5 summarizes the diagnostics used to assess the quality and robustness of the orbital eccentricity imputation. Panel (a) compares the empirical distribution of observed eccentricities with the distribution of imputed values. The close agreement between the two indicates that the imputation procedure preserves the overall shape of the eccentricity distribution and does not introduce artificial modes or inflate the high-eccentricity tail. Panel (b) illustrates the uncertainty associated with each imputed eccentricity, quantified as the standard deviation across bootstrap-based imputations. Uncertainty increases gradually with eccentricity,

reflecting the reduced density of training examples at higher eccentricities rather than numerical instability. This behavior is physically plausible and suggests that the model appropriately expresses lower confidence in sparsely populated regions of parameter space. Panel (c) shows the distribution of test-set MAE across multiple bootstrap imputations. The narrow spread of MAE values demonstrates that the selected gradient boosting regressor yields stable predictive performance and that the imputation results are not sensitive to the particular resampling of the training data. Together, these diagnostics support the reliability of the eccentricity imputation and motivate its use in the subsequent modeling and AL experiments.

After preprocessing and imputation, the final dataset consisted of 5821 planets with complete feature vectors, including all 70 potentially habitable planets. This dataset was used unchanged in all subsequent baseline modeling and AL experiments.

2.4. Evaluation metrics

The planet habitability prediction task considered in this work is formulated as a highly imbalanced binary classification problem, with potentially habitable planets constituting a small minority of the overall sample. As a consequence, standard accuracy alone is not a meaningful indicator of model performance, since a trivial classifier predicting all planets as non-habitable would achieve a deceptively high accuracy. Instead, a set of complementary evaluation metrics (V. Acquaviva 2023) was employed to assess different aspects of classifier behavior, with particular emphasis on sensitivity to the minority class.

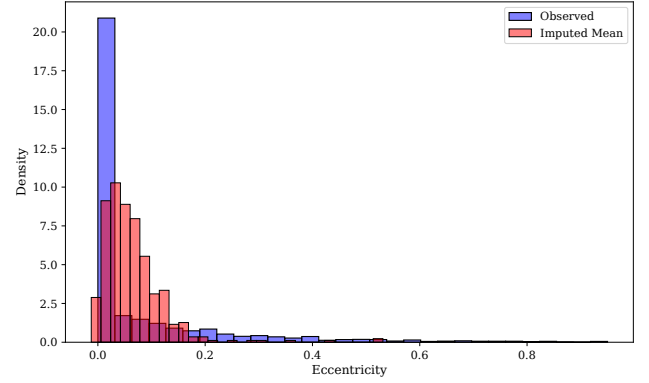
Recall, also referred to as sensitivity or true positive rate, is defined as

$$\text{Recall} = \frac{\text{TP}}{\text{TP} + \text{FN}}, \quad (4)$$

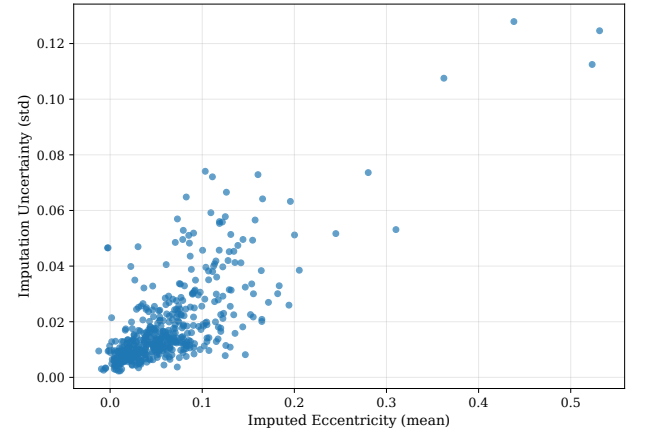
where TP and FN denote the number of true positives and false negatives, respectively. Recall quantifies the fraction of truly potentially habitable planets that are correctly identified by the model. In the present context, recall is of primary importance, as failing to identify a potentially habitable planet represents a more severe error than incorrectly flagging a non-habitable one. Precision measures the reliability of positive predictions and is given by

$$\text{Precision} = \frac{\text{TP}}{\text{TP} + \text{FP}}, \quad (5)$$

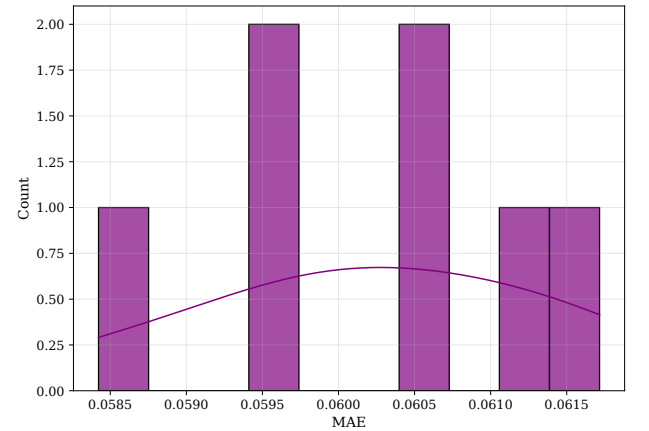
where FP denotes the number of false positives. Precision complements recall by indicating the degree of contamination in the set of planets predicted as potentially habitable. The F1-score is defined as the harmonic



(a)



(b)



(c)

Figure 5. Diagnostics of orbital eccentricity imputation. Panel (a) shows a comparison between the observed eccentricity distribution and the distribution of imputed values, showing close agreement and preservation of the empirical shape; while panel (b) illustrates imputation uncertainty, measured as the standard deviation across bootstrap imputations, as a function of the imputed eccentricity; higher uncertainty at larger eccentricities reflects data sparsity rather than model instability; and panel (c) shows the distribution of test-set MAE across multiple bootstrap imputations, demonstrating stable and consistent predictive performance.

mean of precision and recall,

$$F1 = 2 \times \frac{\text{Precision} \times \text{Recall}}{\text{Precision} + \text{Recall}}, \quad (6)$$

and provides a single scalar summary of performance when a balance between sensitivity and reliability is desired.

To account explicitly for class imbalance, balanced accuracy was also computed. Balanced accuracy is defined as the average of the recall obtained on each class,

$$\text{Balanced Accuracy} = \frac{1}{2} \left(\frac{\text{TP}}{\text{TP} + \text{FN}} + \frac{\text{TN}}{\text{TN} + \text{FP}} \right), \quad (7)$$

where TN denotes true negatives. This metric penalizes classifiers that perform well on the majority class but poorly on the minority class. Finally, the area under the receiver operating characteristic curve (AUROC) (T. Fawcett 2006) was used to assess the ranking quality of probabilistic predictions independently of any fixed classification threshold. The AUROC measures the probability that a randomly chosen potentially habitable planet is assigned a higher predicted probability than a randomly chosen non-habitable one.

Across all experiments, recall was treated as the primary optimization metric, reflecting the scientific objective of minimizing missed potentially habitable planets. The remaining metrics were used to provide a more complete characterization of classifier performance and to facilitate comparisons between different modeling approaches.

2.5. Supervised learning baseline

To establish a strong reference point for subsequent AL experiments, we first evaluated a set of supervised learning models trained on the fully preprocessed dataset described in Section 2.3. These baselines serve two purposes: they quantify the achievable performance under standard passive learning, and they provide a fixed classifier architecture to be used within the AL framework introduced in later sections.

The dataset was divided into training and testing subsets using an 80/20 split, stratified by the habitability label to preserve the strong class imbalance between potentially habitable and non-habitable planets. Stratification ensures that both subsets contain comparable proportions of positive and negative instances, which is essential for meaningful evaluation under imbalance. Three supervised classifiers were considered:

1. Random Forest (RF) (L. Breiman 2001), an ensemble of decision trees trained on bootstrap samples with randomized feature selection, known for

robustness to noise and nonlinear feature interactions.

2. Extreme Gradient Boosting (XGBoost) (T. Chen & C. Guestrin 2016), a gradient-boosted tree ensemble that sequentially fits weak learners to correct previous errors, incorporating regularization and subsampling to control overfitting.
3. Multilayer Perceptron (MLP) (H. A. Bourlard & N. Morgan 1994), a feedforward neural network trained via backpropagation, representing a parametric, non-tree-based alternative.

These models were selected to cover a range of inductive biases and learning paradigms commonly used in astrophysical classification tasks (e.g., C. J. Fluke & C. Jacobs (2019); D. de Andres et al. (2022); A. Agarwal (2023); F. Z. Zeraatgari et al. (2023); S. R. Bhavanam et al. (2024)). All performance evaluation relied on the metrics defined in Section 2.4, with recall treated as the primary criterion due to the scientific importance of minimizing missed potentially habitable planets.

To obtain unbiased estimates of generalization performance while tuning hyperparameters, a nested cross-validation strategy was employed. Nested cross-validation separates hyperparameter optimization from performance estimation and is particularly important when working with limited positive samples. An outer cross-validation loop consisting of five stratified folds repeated five times was used to assess model performance. Within each outer training fold, an inner stratified three-fold cross-validation loop was used to perform grid-based hyperparameter optimization (J. Bergstra & Y. Bengio 2012). For each candidate model, a preprocessing-and-classification pipeline was constructed, consisting of a robust feature scaler followed by the classifier. Robust scaling (P. J. Huber 1981) was chosen to mitigate the influence of outliers and heavy-tailed feature distributions, which are common in exoplanetary and stellar parameters. Hyperparameter grids were explored independently for each model, and model refitting within the inner loop was performed using recall as the selection metric. For each outer fold, the best-performing estimator identified by the inner loop was evaluated on the held-out validation data, and performance metrics were recorded.

Performance metrics obtained from the outer cross-validation folds were aggregated to compare the candidate models in a statistically consistent manner. Model selection was based primarily on recall, with secondary consideration given to stability across folds and complementary metrics such as balanced accuracy and AUROC. Based on this procedure, a single classifier ar-

chitecture and associated hyperparameter configuration were selected as the supervised baseline. This model was subsequently retrained on the full training set using the same preprocessing pipeline. The held-out test set was reserved exclusively for final evaluation and was not used during any stage of model election or hyperparameter tuning. All quantitative results of the cross-validation experiments, final test-set evaluation, and model comparisons are presented in Section 3.1.

To facilitate physical interpretation of the selected baseline model, two complementary feature importance analyses were performed. First, SHAP (SHapley Additive exPlanations) (S. Lundberg & S.-I. Lee 2017) values were computed to quantify the average marginal contribution of each feature to the model’s predictions. SHAP values are grounded in cooperative game theory and provide consistent, model-agnostic explanations of feature influence. Second, permutation importance was computed with respect to recall. In this approach, the values of individual features are randomly permuted while all other features are held fixed, and the resulting change in recall is measured. This method directly assesses the dependence of model sensitivity on each feature. The results of both interpretability analyses are presented and discussed in Section 3.1, alongside the corresponding visualizations.

The supervised learning baseline established in this section provides the fixed classifier architecture used throughout the AL experiments described in Section 2.6. By holding the model architecture constant, differences in performance can be attributed directly to the choice of query strategy rather than to changes in model capacity or optimization procedure.

2.6. Active learning framework and query strategies

AL is employed in this study to reduce the labeling effort required to identify potentially habitable exoplanets by iteratively selecting the most informative candidates for annotation. We adopt a pool-based active learning (D. A. Cohn et al. 1996) setting, which is appropriate when a large collection of unlabeled instances is available and labels are assumed to be costly, as is the case for habitability assessments that typically require detailed observational follow-up.

The final preprocessed dataset described in Sections 2.1 and 2.3 is first divided into disjoint training and test subsets using an 80/20 split, stratified by the habitability label to preserve the severe class imbalance. The test set remains fixed throughout all AL experiments and is never queried or augmented, serving exclusively as an unbiased evaluation set. The training subset is treated as the AL pool, from which labeled and unlabeled sub-

sets are dynamically constructed during each run. At the start of every run, a small labeled seed is sampled from the training data, while the remaining instances constitute the unlabeled pool. This process is repeated independently across multiple runs to assess robustness against random initialization effects.

Seed selection is a critical design choice in AL, particularly under class imbalance. For each run, the initial labeled set consists of a total of 20 instances, including 3 planets labeled as potentially habitable and 17 labeled as non-habitable. This constraint ensures that the classifier is exposed to at least a minimal representation of the positive class from the outset, preventing degenerate early models that fail to identify rare positives. Seed instances are sampled randomly within each class from the training subset, using a different random seed for each run. This strategy balances realism—reflecting limited prior knowledge—with the practical necessity of initializing a usable classifier.

At the beginning of each run, feature scaling is performed using a robust scaler. The scaler is fitted exclusively on the seed set and subsequently applied to the unlabeled pool and the fixed test set, ensuring that no information from unlabeled or test instances leak into the scaling process. The classifier architecture used within the AL loop is fixed to the best-performing supervised model identified by the steps described in Section 2.5 with tuned hyperparameters. At each iteration, the model is retrained from scratch on the expanded labeled set to reflect the updated training distribution.

Two query strategies are considered in this work: random sampling and margin sampling. Random sampling serves as a baseline, in which unlabeled instances are selected uniformly at random from the pool. Although simple, this strategy provides a reference against which the effectiveness of more informed querying can be evaluated. Margin sampling (M.-F. Balcan et al. 2007) is an uncertainty-based strategy that selects the instance for which the classifier is least confident. For probabilistic binary classifiers, this is quantified as the absolute difference between the predicted class probabilities. Instances with small margins lie closest to the decision boundary and are therefore expected to be the most informative for refining the classifier. Margin sampling represents a purely exploitative strategy, focusing on regions of maximal uncertainty in the current model. Both strategies operate within the same AL loop and are evaluated under identical conditions to ensure a fair comparison.

For each run and each query strategy, the AL process proceeds iteratively for a fixed labeling budget of 70 queried instances. At every iteration, a single unlabeled instance is selected according to the AL strategy,

removed from the pool, added to the labeled set along with its true label, and the classifier is retrained. Model performance is not evaluated after every query but instead recorded at regular intervals of five newly labeled instances. This aggregation interval reduces noise in the learning curves while preserving temporal resolution sufficient to capture performance trends. The stopping criterion is therefore budget-based rather than performance based, allowing learning trajectories to be compared across strategies. To account for stochastic variability arising from seed selection and model training, the entire procedure is repeated across 20 independent runs. Performance metrics are averaged across runs at each evaluation point, yielding mean learning curves and associated variability estimates.

At the conclusion of each run, the final trained model and its associated scaler are saved. These persisted models are subsequently reused for downstream analysis, including ensemble-based probability aggregation and planet recommendation, which are described in Section 2.7. Importantly, this reuse does not affect the AL process itself, as all querying and evaluation decisions are completed prior to model persistence.

2.7. Planet recommendation via ensemble uncertainty

Beyond performance evaluation, an important objective of this study is to demonstrate how the trained models can be used to prioritize exoplanets for further observational follow-up. To this end, we formulate planet recommendation as a probabilistic ranking problem that explicitly accounts for model uncertainty arising from limited labeled data and stochastic training effects.

In the context of exoplanet habitability, false negatives are particularly costly, as potentially habitable planets may be overlooked due to incomplete or noisy measurements. Consequently, rather than relying on a single deterministic model prediction, we adopt an ensemble-based probabilistic approach that aggregates information across multiple independently trained models. Each AL run produces a final classifier trained on a distinct labeled set obtained through different random seeds and query trajectories. These models represent alternative hypothesis consistent with the data and the AL process. Their collective behavior provides a natural mechanism for quantifying uncertainty due to limited labeled data.

For each completed AL run, the final trained classifier and its associated feature scaler are retained. All retained models are subsequently applied to the entire dataset, including both the originally labeled instances and the remaining planets labeled as non-habitable in the catalog. Feature scaling is performed using the scaler associated with each individual model to preserve

consistency with the model’s training distribution. For a given planet, this procedure yields a set of predicted habitability probabilities, one from each model in the ensemble. No model refitting or additional calibration is performed at this stage.

The ensemble predictions are summarized using two statistics: the mean predicted probability and the standard deviation across models. The mean probability serves as an estimate of the model-averaged likelihood that a planet belongs to the potentially habitable class, while the standard deviation provides a measure of uncertainty associated with this estimate. A high mean probability accompanied by low variability across models indicates a robust recommendation, whereas large variability suggests sensitivity to training data composition and reduced confidence. This distinction is particularly important when prioritizing targets for follow-up observations under constrained observational resources.

To focus the recommendation process on genuinely novel targets, only planets labeled as non-habitable in the original catalog are considered at this stage. These planets are ranked in descending order according to their ensemble-averaged habitability probability. No hard probability threshold is imposed a priori. Instead, the ranked list is inspected to identify planets that simultaneously exhibit elevated predicted habitability and relatively low ensemble uncertainty. This approach avoids overconfidence in marginal cases while retaining flexibility in defining follow-up priorities based on available resources or scientific objectives.

It is important to emphasize that the recommendation procedure does not assert definitive habitability. Rather, it provides a data-driven prioritization informed by the learned relationships in the available feature space. The resulting candidates should be interpreted as targets for further study, where additional observational constraints may confirm or refute their habitability status. Moreover, the recommendations are inherently conditioned on the choice of features, preprocessing steps, and labeling assumptions described in earlier sections. As such, they should be considered complementary to, rather than a replacement for, domain-driven assessment and physical modeling.

3. RESULTS

3.1. Supervised baseline performance

We first establish supervised learning baselines to quantify the achievable performance under a conventional, fully supervised setting before introducing AL. These baselines serve two purposes: (i) they provide an upper reference for label efficiency comparisons, and (ii) they determine the classifier architecture used in subse-

quent AL experiments. Three supervised classifiers were evaluated: RF, XGBoost, and MLP. To obtain robust performance estimates under severe class imbalance, we employed nested cross-validation, in which an inner loop performs hyperparameter tuning while an outer loop estimates generalization performance. Both loops were stratified by the habitability label to preserve class proportions. Performance was assessed primarily using recall, defined as the fraction of potentially habitable planets correctly identified. This choice reflects the scientific objective of minimizing false negatives—i.e., missing genuinely interesting targets—while secondary metrics (precision, F1-score, balanced accuracy, and AUROC) were retained for diagnostic completeness. Balanced accuracy, defined as the mean of recall for the positive and negative classes, mitigates bias toward the dominant non-habitable class, while AUROC summarizes ranking performance across decision thresholds. Across repeated outer folds, XGBoost consistently achieved the highest mean recall, followed by RF, with the MLP showing both lower performance and substantially higher variance. These results indicate that tree-based ensemble methods are better suited to the heterogeneous feature scales and nonlinear dependencies present in the dataset. The MLP’s sensitivity to limited positive samples and hyperparameter initialization likely contributes to its inferior stability.

To contextualize model performance beyond recall alone, we compare the three supervised classifiers across all evaluation metrics using a radar (spider) plot (Figure 6). This visualization highlights the trade-offs between sensitivity, precision, and overall discrimination. While RF performs competitively on precision and balanced accuracy, XGBoost achieves the most favorable balance across all metrics simultaneously. The MLP underperforms consistently, particularly in recall and balanced accuracy, confirming its unsuitability as a baseline in this setting. Given these results, XGBoost is adopted as the reference supervised learner for all subsequent AL experiments.

The optimal configuration favored shallow trees and moderate subsampling, consistent with controlling overfitting in a low-signal, high-imbalance regime. The selected hyperparameters were a maximum tree depth of three, subsample and column-subsample fractions of 0.8, and a learning rate of 0.1. The model was then retrained on the full training set using these hyperparameters and evaluated once on a held-out test set that was not used during any stage of model selection. The quantitative performance of the final XGBoost model on the held-out test set is summarized in Table 1. It demonstrates high sensitivity to potentially habitable planets, while

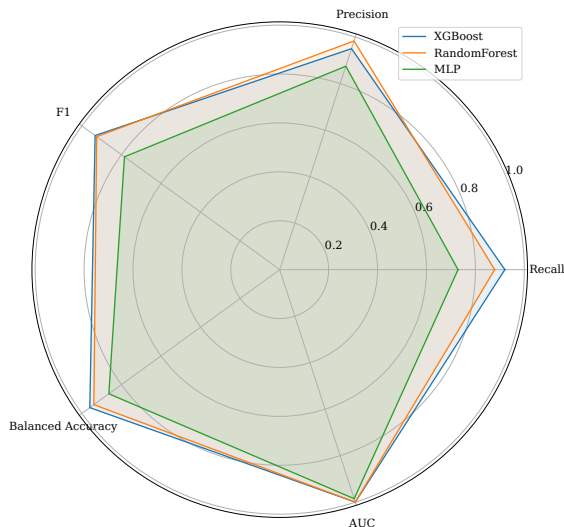


Figure 6. Radar plot comparing supervised classifiers across recall, precision, F1-score, balanced accuracy, and AUROC. XGBoost exhibits the strongest overall performance and is selected as the baseline model.

Table 1. Performance of the final XGBoost classifier evaluated on the held-out test set. Metrics are defined in Section 2.4.

Metric	Value
Recall	0.929
Precision	0.929
F1-score	0.929
Balanced accuracy	0.964
AUROC	0.999

maintaining excellent discrimination overall, as reflected by the near-unity AUROC. These results establish XGBoost as a strong supervised reference and justify its use as the base learner in the AL framework described in Section 2.6. It is noteworthy that recall, precision, and F1-score take identical numerical values for the final XGBoost model. This occurs because, at the selected operating point on the held-out test set, the number of false positives and false negatives is equal, yielding identical values for precision and recall. Since the F1-score is defined as the harmonic mean of precision and recall, it reduces to the same value under these conditions. This equality is therefore a consequence of the specific confusion-matrix configuration induced by the decision threshold, rather than an artifact of the evaluation process.

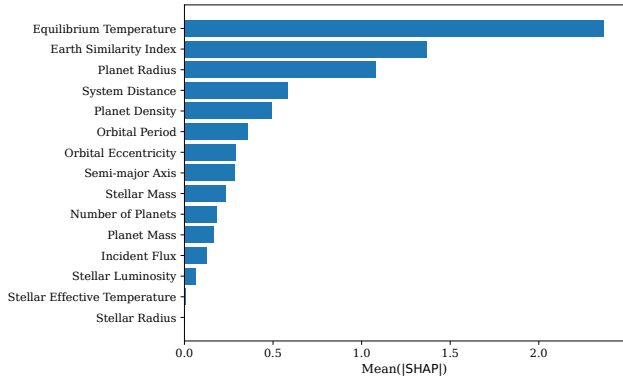


Figure 7. Global feature importance based on mean absolute SHAP values for the XGBoost classifier. Features are ordered by decreasing contribution to the model output, highlighting the dominant role of thermal and habitability-related parameters.

To interpret the predictions of the selected XGBoost model, we employed two complementary feature importance techniques. First, SHAP values were used to quantify the average marginal contribution of each feature to the model output. SHAP is grounded in cooperative game theory and provides consistent, model-agnostic attributions. The global SHAP summary (Figure 7) indicates that planetary equilibrium temperature and ESI dominate the model’s decision process, followed by planetary radius and system distance. Orbital parameters and stellar properties contribute more weakly but non-negligibly. Second, permutation importance was computed with respect to recall by randomly shuffling individual features and measuring the resulting decrease in recall. This method directly assesses a feature’s importance for the specific scientific objective of recovering potentially habitable planets. The permutation results (Figure 8) reinforce the SHAP findings, highlighting equilibrium temperature and ESI as the most critical predictors for recall, with a steep performance drop when either feature is disrupted. The consistency between SHAP and permutation importance increases confidence that the model relies on physically meaningful quantities rather than spurious correlations.

3.2. Active learning performance

To evaluate the effectiveness of AL relative to passive data acquisition, we compared a random sampling baseline with an uncertainty-driven margin sampling strategy using the same classifier architecture, initialization, and evaluation protocol. All results reported in this section are aggregated over 20 independent runs with different random seeds to mitigate stochastic effects arising from seed selection and model initialization. The

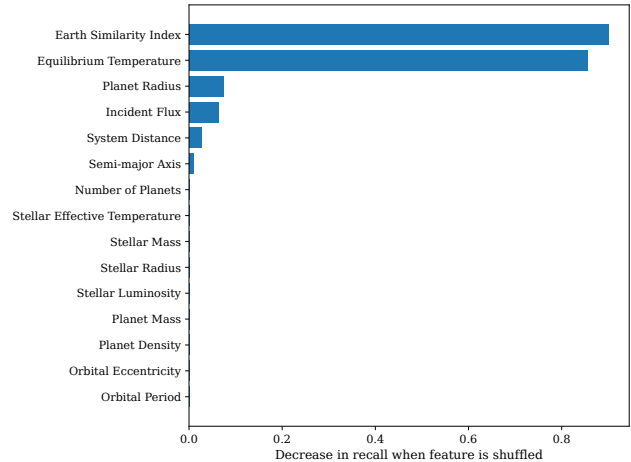


Figure 8. Permutation feature importance measured as the decrease in recall when individual features are randomly shuffled. Larger values indicate greater importance for identifying potentially habitable planets.

learning dynamics are summarized in Figure 9, which shows the evolution of recall, precision, F1-score, and balanced accuracy as a function of the number of labeled instances. Shaded regions indicate the inter-run variability, quantified as one standard deviation around the mean. Performance is reported every five queried instances to reduce noise and to emphasize trends at a scale relevant for annotation budgeting.

From the earliest stages of the learning process, margin-based querying substantially outperforms random sampling in terms of recall. With only 20 labeled instances (the initial seed set), both strategies start from comparable performance levels. However, after a small number of AL queries, the margin strategy rapidly identifies informative samples near the classifier’s decision boundary, leading to a sharp increase in recall. The early-recall statistic, computed after the first evaluation interval, reaches 0.925 for margin sampling compared to 0.459 for random sampling, demonstrating a more than twofold improvement in the recovery of potentially habitable planets under severe label scarcity. As additional instances are acquired, the superiority of margin sampling persists across all reported metrics. Precision and F1-score increase steadily, indicating that the gain in recall is not achieved at the expense of excessive false positives. By the later stages of the budget, the margin strategy converges to high and stable performance, with late-stage precision and F1-scores both reaching approximately 0.929. In contrast, random sampling exhibits slower improvement and substantially larger variance across runs, reflecting its inefficiency in prioritizing informative observations in an imbalanced setting.

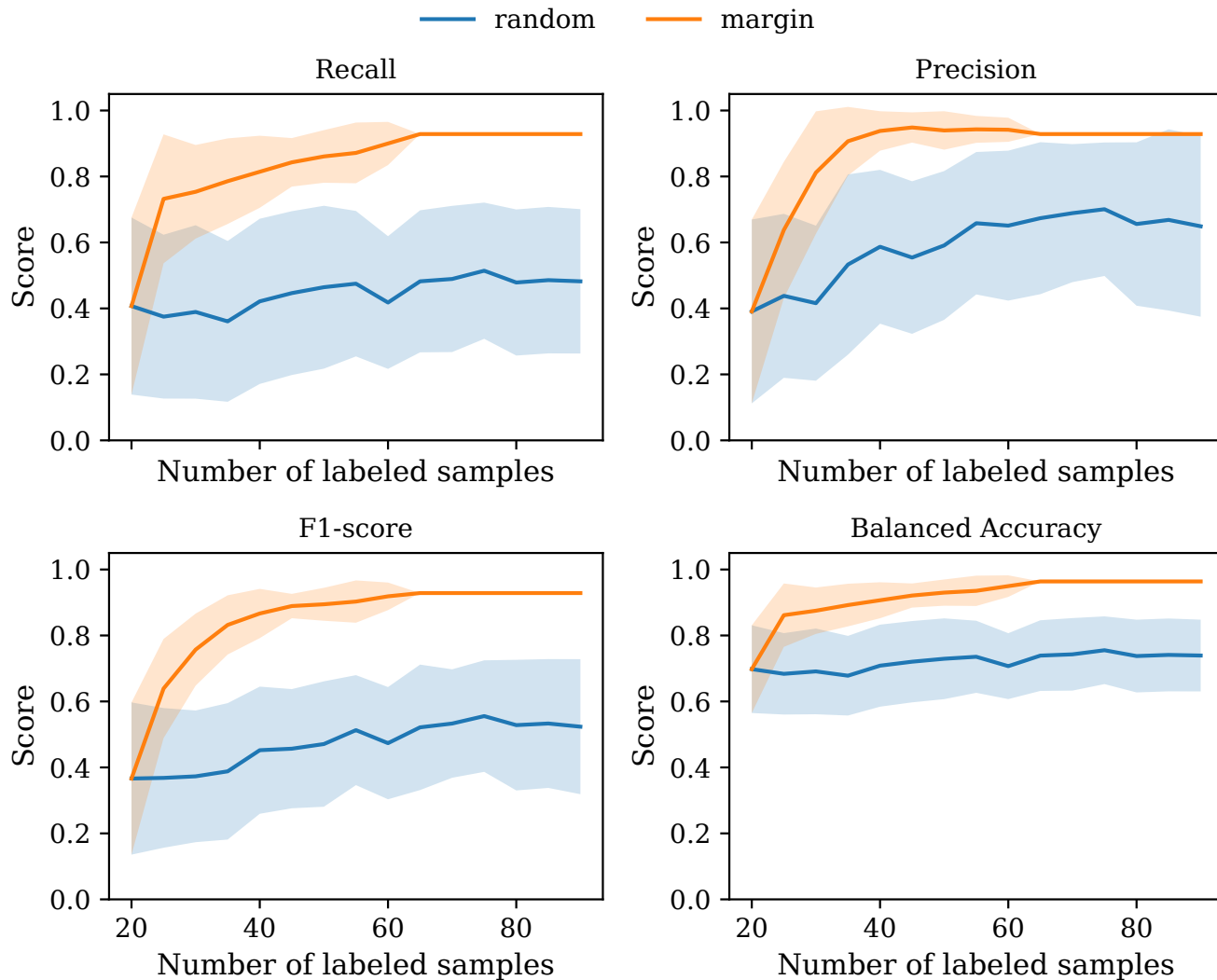


Figure 9. Active learning performance as a function of the number of labeled instances. Mean learning curves over 20 independent runs, evaluated every five queried instances. Shaded regions indicate ± 1 standard deviation across runs, illustrating inter-run variability.

Balanced accuracy, which accounts for both sensitivity and specificity under class imbalance, further highlights the benefits of active querying. The margin strategy attains a late-stage balanced accuracy of 0.964, whereas random sampling remains below 0.741 even after exhausting the labeling budget. This divergence indicates that uncertainty-based querying enables the classifier to learn a more symmetric decision boundary with respect to habitable and non-habitable classes, despite the strong class skew in the dataset. An important qualitative feature of the learning curves is the early saturation of the margin strategy. After approximately 60–65 labeled instances, performance gains plateau across all metrics, suggesting that the model has already captured the most informative structure available in the fea-

ture space. This behavior is consistent with the notion that, for this problem, a relatively small but carefully selected subset of planets is sufficient to approach the performance achieved with substantially larger labeled samples.

Overall, these results demonstrate that AL, when combined with an uncertainty-based query strategy, can dramatically accelerate model improvement in the low-label regime relevant to exoplanet habitability studies. The margin sampler not only improves final performance, but importantly, reaches high recall and balanced accuracy using a fraction of the labeled data required by random sampling. The implications of this efficiency in terms of computational cost and practical deployment are examined in the following subsection.

3.3. Efficiency of active learning

While the previous section focused on comparative predictive performance, the principal advantage of AL in this study lies in its label efficiency: the ability to reach high-quality habitability classification with substantially fewer labeled instances. This distinction is particularly important in the exoplanet domain, where positive labels are rare and expensive to refine observationally. As shown in Figure 9, margin-based uncertainty sampling exhibits rapid performance gains in the early stages of learning, achieving high recall and balanced accuracy after only a limited number of queried instances. In contrast, random sampling improves more gradually and does not reach a comparable performance regime within the labeling budget explored in this study. This divergence highlights the inefficiency of passive sampling under severe class imbalance, where randomly selected instances are unlikely to be informative for the minority class.

The efficiency gain of margin sampling is most evident in recall and F1-score, both of which increase sharply during the initial acquisition phase and stabilize thereafter. Importantly, this behavior indicates that the model quickly learns a meaningful decision boundary for potentially habitable planets, rather than merely increasing positive predictions indiscriminately. Random sampling, by comparison, continues to exhibit slow and noisy improvement across all metrics, with substantial variance across runs. From a practical standpoint, these results imply that uncertainty-driven AL can substantially reduce the number of labeled planets required to achieve scientifically useful classification performance. This reduction directly translates into lower dependence on large annotated catalogs and fewer iterations of model retraining before deployment. The reduced inter-run variability observed for margin sampling further suggests greater robustness to the specific choice of initial seed set, an important consideration in small-sample astrophysical problems.

In summary, margin-based AL demonstrates a clear efficiency advantage over random sampling by concentrating label queries in regions of maximal informational value. Within the investigated budget, it consistently outperforms passive learning and reaches a stable, high performance regime that random sampling fails to attain, thereby justifying its use in subsequent ensemble-based planet recommendation. At the largest labeling budgets explored, the margin-based AL strategy approaches, but does not fully exceed, the performance of the supervised XGBoost baseline trained on the full labeled dataset, which will be further discussed in Section 4.

3.4. Planet recommendation

To translate the outcomes of the AL framework into an astronomically meaningful product, we applied the ensemble of trained classifiers to the full preprocessed dataset. Each classifier was used to predict the habitability probability for every planet after scaling the input features with its associated preprocessing pipeline. This resulted in a set of predicted probabilities per planet, one from each independently trained model. For each planet, we aggregated these predictions by computing the mean predicted habitability probability and its standard deviation, which serves as a measure of model-induced uncertainty. To focus on genuinely novel recommendations, we restricted this analysis to planets labeled as non-habitable in the HWC.

The ranked list of candidates revealed a single planet that clearly separated from the rest of the non-habitable population. This exoplanet exhibited a mean predicted habitability probability of 0.82 with a standard deviation of 0.06 across the ensemble, while remaining candidates showed substantially lower mean probabilities (≤ 0.30). The combination of a high mean score and relatively low dispersion indicates a consistent model response rather than sensitivity to individual training realizations.

Cross-matching this candidate against the merged dataset of the HWC and the PSCompPars table using tolerance-based matching on orbital, planetary, and stellar parameters yielded a unique identification: τ Ceti f, a planet orbiting the nearby G-type (M. C. Turnbull 2015) star τ Ceti at a distance of 3.6 pc (K. G. Stassun et al. 2019). τ Ceti f was discovered via the radial-velocity method in 2017 and resides in a multi-planet system with four known planets (F. Feng et al. 2017). The physical parameters of τ Ceti f place it close to the central tendency of the potentially habitable sample in several dimensions. Its planetary radius ($1.81R_{\oplus}$) and mass ($3.93M_{\oplus}$) are consistent with the upper range of super-Earths, while its orbital semi-major axis (1.33 AU) and equilibrium temperature (≈ 185 K) fall within the broad distribution spanned by cataloged potentially habitable planets. A comparison with the median and interquartile range of the potentially habitable population is provided in Table 2.

Inspection of instance-level SHAP values further indicates that elevated habitability score of τ Ceti f is primarily driven by its incident stellar flux, planetary radius, and equilibrium temperature, with secondary contributions from orbital eccentricity and system distance. These factors collectively shift the model output toward the positive class despite the planet’s exclusion from the catalog’s potentially habitable designation.

Table 2. Comparison between the recommended planet (τ Ceti f) and the distribution of cataloged potentially habitable planets. For each parameter, the value of the recommended candidate is shown alongside the median and interquartile range (IQR) of the potentially habitable sample.

<i>Planetary and orbital parameters</i>			
Parameter	Candidate	Median	IQR
Orbital period (days)	636.13	36.77	92.30
Semi-major axis (AU)	1.334	0.165	0.290
Orbital eccentricity	0.160	0.083	0.141
Planet radius (R_{\oplus})	1.81	1.78	0.90
Planet mass (M_{\oplus})	3.93	4.06	3.48
Planet density (g cm^{-3})	0.66	0.68	0.46
Incident flux (S_{\oplus})	0.28	0.85	0.68
Equilibrium temperature (K)	184.7	244.0	47.4
Earth Similarity Index	0.555	0.729	0.169
<i>Host star and system parameters</i>			
Stellar T_{eff} (K)	5310	3460	919.5
Stellar mass (M_{\odot})	0.78	0.42	0.36
Stellar radius (R_{\odot})	0.83	0.42	0.34
Stellar luminosity (L_{\odot})	0.50	0.023	0.072
System distance (pc)	3.60	31.13	241.09
Planets in system	4	2	2

Importantly, this recommendation does not constitute a reclassification of τ Ceti f as habitable. Instead, it demonstrates how an ensemble-based AL framework can be used to prioritize specific planets for further observational or theoretical investigation, particularly when predictions are both high-confidence and robust to model uncertainty. In this sense, τ Ceti f serves as a concrete example of how AL-driven prioritization can complement existing catalogs and guide follow-up efforts.

4. DISCUSSION

This study investigated the use of AL for exoplanet habitability classification under conditions of extreme class imbalance and label uncertainty. By combining a carefully constructed feature set, a strong supervised baseline, and uncertainty-driven AL strategies, we evaluated both predictive performance and label efficiency, and demonstrated a concrete downstream application in the form of planet recommendation. Below, we discuss the implications of these findings, their relevance to habitability studies, and the limitations that contextualize the conclusions.

The results presented in Section 3.2 demonstrate that margin-based AL substantially outperforms random sampling throughout the labeling process, particularly in the low-label regime most relevant to astronom-

ical follow-up. The early-recall improvement observed for margin sampling highlights a central strength of uncertainty-based AL: the ability to focus labeling effort on ambiguous regions of feature space where the classifier’s decision boundary is poorly constrained. Under extreme class imbalance, such regions are disproportionately informative for identifying rare positive instances. An important qualitative feature of the learning curves is the rapid saturation of margin sampling relative to random sampling. Performance gains plateau after approximately 60–65 labeled instances, suggesting that the majority of discriminative information relevant to habitability classification is captured early when queries are selected adaptively. In contrast, random sampling does not achieve comparable performance within the same labeling budget, reflecting its inefficiency in discovering informative minority-class examples when positives are sparse. Notably, margin sampling approaches—but does not exceed—the performance of the fully supervised XGBoost baseline trained on the entire training set. This behavior is expected: AL does not introduce new information beyond what is present in the data, but instead reorders label acquisition. The convergence of AL performance toward the supervised upper bound therefore supports the interpretation that AL achieves label efficiency rather than absolute performance gains, reaching near-supervised performance with substantially fewer labeled instances.

From an astrophysical perspective, the results reinforce the view that habitability assessment is inherently multivariate and cannot be reduced to simple thresholding on individual parameters. The substantial overlap between potentially habitable and non-habitable planets in marginal feature distributions (Figure 4) explains why uncertainty-driven AL is particularly effective: planets near the decision boundary are both common and informative, and querying them accelerates learning. The dominance of equilibrium temperature, incident stellar flux, and ESI in both SHAP and permutation importance analyses suggests that the models largely recover physically meaningful relationships already encoded—implicitly or explicitly—in habitability heuristics. However, the presence of secondary contributions from orbital eccentricity, system distance, and planetary bulk properties indicates that the classifier integrates multiple weak signals rather than relying on a single proxy. This behavior is desirable in a prioritization context, where incomplete or uncertain measurements are the norm. Importantly, the AL framework demonstrated here does not attempt to redefine habitability. Instead, it provides a principled mechanism for prioritizing planets that are ambiguous under current catalog definitions.

In this sense, AL aligns naturally with observational practice: it identifies targets where additional data are most likely to refine scientific understanding, rather than reinforcing already well-separated cases.

The ensemble-based recommendation of τ Ceti f illustrates the conservative character of the proposed framework. Despite evaluating thousands of non-habitable-labeled planets, only a single candidate emerges with both a high mean predicted habitability probability and low-model uncertainty. This outcome reflects the combined effects of severe class imbalance, cautious aggregation across independently trained models, and the requirement for consistency rather than isolated high scores. Such conservatism is a feature rather than a limitation in the context of follow-up prioritization. False positives in habitability studies can divert scarce observational resources, whereas false negatives can often be revisited as catalogs evolve. By emphasizing robustness across models and explicitly quantifying uncertainty, the recommendation procedure favors candidates whose prioritization is stable under variations in training data and AL trajectories. The identification of τ Ceti f—already a well-studied planet in a nearby system (F. Feng et al. 2017)—also highlights an important interpretive point: the framework is not designed to discover exotic outliers, but rather to reassess borderline cases in light of learned multivariate patterns. The agreement between the candidate’s properties and the central tendencies of the potentially habitable population (Table 2) emphasizes this role as a prioritization aid rather than a discovery engine.

Several limitations should be borne in mind when interpreting the results. First, the habitability labels used throughout the study are heuristic and literature-derived, rather than direct indicators of biological or even surface habitability. While AL is robust to some degree of label noise, systematic biases in catalog definitions inevitably propagate into the learned models. Second, the feature set, while physically motivated, is constrained by current data availability. Atmospheric composition, obliquity, magnetic fields, and long-term climate stability are not represented, yet are critical to habitability. The conclusions therefore apply strictly within the scope of the adopted features and should not be extrapolated beyond them. Third, the AL simulations assume oracle access to true labels during querying. In practice, follow-up observations yield partial, delayed, or uncertain information rather than binary labels. Extending the framework to incorporate probabilistic or multi-fidelity labels represents an important direction for future work. Finally, the recommendation results are conditioned on the specific classifier architec-

ture (XGBoost) and query strategy (margin sampling) selected in this study. While the consistency of results across runs suggest robustness, alternative models or strategies could yield different prioritization, particularly as new data become available.

5. CONCLUSIONS

In this work, we investigated the use of AL to accelerate habitability classification in exoplanet catalogs characterized by extreme class imbalance, heterogeneous data quality, and uncertain labels. By combining physically motivated feature selection, careful preprocessing, and a robust supervised baseline with uncertainty-driven query strategies, we demonstrated that AL can substantially reduce the number of labeled instances required to achieve near-supervised performance.

We first established a strong supervised baseline using gradient-boosted decision trees, evaluated under repeated nested cross-validation and optimized for recall to reflect the scientific priority of identifying rare potentially habitable planets. Feature-importance analyses based on SHAP values and permutation testing showed that the model relies primarily on physically interpretable parameters such as equilibrium temperature, stellar irradiance, planetary radius, and ESI, while integrating secondary orbital and system-level features in a complementary manner. Building on this baseline, we implemented a pool-based AL framework and compared random sampling with margin-based querying across multiple runs and labeling budgets. Margin sampling consistently outperformed random selection, particularly in the low-budget regime, achieving rapid gains in recall and balanced accuracy with only a fraction of the labeled data required by passive learning. These results confirm that uncertainty-driven querying is well suited to habitability classification, where informative instances tend to cluster near poorly constrained decision boundaries.

Beyond performance evaluation, we demonstrated a practical downstream application of the AL framework by aggregating predictions from multiple trained models to recommend candidates for further observational study. By ranking non-habitable-labeled planets according to ensemble mean probability and associated uncertainty, we identified a single robust candidate— τ Ceti f—with a high predicted habitability probability and low inter-model variance. This result illustrates how AL outputs can be translated into conservative, uncertainty-aware prioritization rather than speculative discovery claims.

Overall, this study shows that AL provides a principled and computationally tractable approach for guid-

ing follow-up efforts in exoplanet science, particularly as catalogs continue to grow faster than observational resources. While the conclusions are necessarily conditioned on heuristic habitability labels and currently available features, the proposed framework is readily extensible to future datasets, alternative classifiers, and more nuanced labeling schemes. As exoplanet surveys expand in scale and complexity, integrating AL into catalog analysis pipelines offers a promising path toward more efficient and transparent scientific decision-making.

ACKNOWLEDGMENTS

This research has made use of the NASA Exoplanet Archive, which is operated by the California Institute

of Technology, under contract with the National Aeronautics and Space Administration under the Exoplanet Exploration Program.

Facility: Exoplanet Archive

Software: numpy (S. van der Walt et al. 2011), scipy (P. Virtanen et al. 2020), scikit-learn (F. Pedregosa et al. 2011), xgboost (T. Chen & C. Guestrin 2016), shap (S. Lundberg & S.-I. Lee 2017), matplotlib (J. D. Hunter 2007), upsetplot (J. Nothman 2018), seaborn (M. Waskom 2021), modAL (T. Danka & P. Horvath 2018)

REFERENCES

- Acquaviva, V. 2023, Machine learning for physics and astronomy (Princeton: Princeton University Press)
- Agarwal, A. 2023, ApJ, 946, 109, doi: [10.3847/1538-4357/acbdfa](https://doi.org/10.3847/1538-4357/acbdfa)
- Balcan, M.-F., Broder, A., & Zhang, T. 2007, Margin Based Active Learning (Springer Berlin Heidelberg), 35–50, doi: [10.1007/978-3-540-72927-3_5](https://doi.org/10.1007/978-3-540-72927-3_5)
- Barnes, R., Meadows, V. S., & Evans, N. 2015, ApJ, 814, 91, doi: [10.1088/0004-637x/814/2/91](https://doi.org/10.1088/0004-637x/814/2/91)
- Basak, S., Mathur, A., Theophilus, A. J., Deshpande, G., & Murthy, J. 2021, EPJ ST, 230, 2221, doi: [10.1140/epjs/s11734-021-00203-z](https://doi.org/10.1140/epjs/s11734-021-00203-z)
- Bergstra, J., & Bengio, Y. 2012, J. Mach. Learn. Res., 13, 281. <https://api.semanticscholar.org/CorpusID:15700257>
- Bhavanam, S. R., Channappayya, S. S., P. K, S., & Desai, S. 2024, Ap&SS, 369, doi: [10.1007/s10509-024-04357-9](https://doi.org/10.1007/s10509-024-04357-9)
- Bourlard, H. A., & Morgan, N. 1994, Multilayer Perceptrons (Springer US), 59–80, doi: [10.1007/978-1-4615-3210-1_4](https://doi.org/10.1007/978-1-4615-3210-1_4)
- Breiman, L. 2001, Mach. Learn., 45, 5, doi: [10.1023/a:1010933404324](https://doi.org/10.1023/a:1010933404324)
- Chen, T., & Guestrin, C. 2016, in Proceedings of the 22nd ACM SIGKDD International Conference on Knowledge Discovery and Data Mining, KDD '16 (ACM), 785–794, doi: [10.1145/2939672.2939785](https://doi.org/10.1145/2939672.2939785)
- Christiansen, J. L., McElroy, D. L., Harbut, M., et al. 2025, Planet. Sci. J., 6, 186, doi: [10.3847/psj/ade3c2](https://doi.org/10.3847/psj/ade3c2)
- Cohn, D. A., Ghahramani, Z., & Jordan, M. I. 1996, JAIR, 4, 129, doi: [10.1613/jair.295](https://doi.org/10.1613/jair.295)
- Danka, T., & Horvath, P. 2018, doi: [10.48550/ARXIV.1805.00979](https://doi.org/10.48550/ARXIV.1805.00979)
- de Andres, D., Yepes, G., Sembolini, F., et al. 2022, MNRAS, 518, 111, doi: [10.1093/mnras/stac3009](https://doi.org/10.1093/mnras/stac3009)
- Dhama, R., Singh, P. P., & Kumar, V. 2025, in 2025 8th International Conference on New Media Studies (CONMEDIA) (IEEE), 23–28, doi: [10.1109/conmedia67140.2025.11290119](https://doi.org/10.1109/conmedia67140.2025.11290119)
- El-Kholy, R., & Hayman, Z. 2025, A&A, doi: [10.1051/0004-6361/202451309](https://doi.org/10.1051/0004-6361/202451309)
- Fawcett, T. 2006, Pattern Recognit. Lett., 27, 861, doi: [10.1016/j.patrec.2005.10.010](https://doi.org/10.1016/j.patrec.2005.10.010)
- Feng, F., Tuomi, M., Jones, H. R. A., et al. 2017, AJ, 154, 135, doi: [10.3847/1538-3881/aa83b4](https://doi.org/10.3847/1538-3881/aa83b4)
- Fluke, C. J., & Jacobs, C. 2019, WIREs DMKD, 10, doi: [10.1002/widm.1349](https://doi.org/10.1002/widm.1349)
- Hoyle, B., Paeck, K., Rau, M. M., Seitz, S., & Weller, J. 2016, MNRAS, 458, 4498, doi: [10.1093/mnras/stw563](https://doi.org/10.1093/mnras/stw563)
- Huber, P. J. 1981, Robust Statistics (Wiley), doi: [10.1002/0471725250](https://doi.org/10.1002/0471725250)
- Hunter, J. D. 2007, Comput. Sci. Eng., 9, 90, doi: [10.1109/mcse.2007.55](https://doi.org/10.1109/mcse.2007.55)
- Ishida, E. E. O., Beck, R., González-Gaitán, S., et al. 2018, MNRAS, 483, 2, doi: [10.1093/mnras/sty3015](https://doi.org/10.1093/mnras/sty3015)
- Ishida, E. E. O., Kornilov, M. V., Malanchev, K. L., et al. 2021, A&A, 650, A195, doi: [10.1051/0004-6361/202037709](https://doi.org/10.1051/0004-6361/202037709)
- Kennamer, N., Ishida, E. E. O., Gonzalez-Gaitan, S., et al. 2020, in 2020 IEEE Symposium Series on Computational Intelligence (SSCI) (IEEE), 3115–3124, doi: [10.1109/ssci47803.2020.9308300](https://doi.org/10.1109/ssci47803.2020.9308300)
- Kopparapu, R. K., Ramirez, R. M., SchottelKotte, J., et al. 2014, ApJ, 787, L29, doi: [10.1088/2041-8205/787/2/L29](https://doi.org/10.1088/2041-8205/787/2/L29)

- Leoni, M., Ishida, E. E. O., Peloton, J., & Möller, A. 2022, *A&A*, 663, A13, doi: [10.1051/0004-6361/202142715](https://doi.org/10.1051/0004-6361/202142715)
- Lex, A., Gehlenborg, N., Strobel, H., Vuillemot, R., & Pfister, H. 2014, *IEEE Transactions on Visualization and Computer Graphics*, 20, 1983, doi: [10.1109/tvcg.2014.2346248](https://doi.org/10.1109/tvcg.2014.2346248)
- Lochner, M., & Bassett, B. 2021, *Astron. Comput.*, 36, 100481, doi: [10.1016/j.ascom.2021.100481](https://doi.org/10.1016/j.ascom.2021.100481)
- Lundberg, S., & Lee, S.-I. 2017, doi: [10.48550/ARXIV.1705.07874](https://doi.org/10.48550/ARXIV.1705.07874)
- Masters, D., Capak, P., Stern, D., et al. 2015, *ApJ*, 813, 53, doi: [10.1088/0004-637x/813/1/53](https://doi.org/10.1088/0004-637x/813/1/53)
- Nothman, J. 2018, upsetplot: A Python implementation of UpSet plots,, <https://github.com/jnothman/UpSetPlot>
- Patel, Y. 2024, Predicting Exoplanets Habitability: Metrics and Models (IntechOpen), doi: [10.5772/intechopen.1007686](https://doi.org/10.5772/intechopen.1007686)
- Pedregosa, F., Varoquaux, G., Gramfort, A., et al. 2011, *J. Mach. Learn. Res.*, 12, 2825–2830
- PHL @ UPR Arcibo. 2025, The Habitable Worlds Catalog (HWC),, <http://phl.upr.edu/hwc>
- Quan, Y., Zhong, X., Feng, W., et al. 2021, *Remote Sens.*, 13, 464, doi: [10.3390/rs13030464](https://doi.org/10.3390/rs13030464)
- Richards, J. W., Starr, D. L., Brink, H., et al. 2011, *ApJ*, 744, 192, doi: [10.1088/0004-637x/744/2/192](https://doi.org/10.1088/0004-637x/744/2/192)
- Rodríguez-Mozos, J. M., & Moya, A. 2017, *MNRAS*, 471, 4628, doi: [10.1093/mnras/stx1910](https://doi.org/10.1093/mnras/stx1910)
- Saha, S., Basak, S., Safonova, M., et al. 2018, *Astron. Comput.*, 23, 141, doi: [10.1016/j.ascom.2018.03.003](https://doi.org/10.1016/j.ascom.2018.03.003)
- Saha, S., Nagaraj, N., Mathur, A., Yedida, R., & H R, S. 2020, *EPJ ST*, 229, 2629, doi: [10.1140/epjst/e2020-000098-9](https://doi.org/10.1140/epjst/e2020-000098-9)
- Schulze-Makuch, D., Méndez, A., Fairén, A. G., et al. 2011, *AsBio*, 11, 1041, doi: [10.1089/ast.2010.0592](https://doi.org/10.1089/ast.2010.0592)
- Solorio, T., Fuentes, O., Terlevich, R., & Terlevich, E. 2005, *MNRAS*, 363, 543, doi: [10.1111/j.1365-2966.2005.09456.x](https://doi.org/10.1111/j.1365-2966.2005.09456.x)
- Stassun, K. G., Oelkers, R. J., Paegert, M., et al. 2019, *AJ*, 158, 138, doi: [10.3847/1538-3881/ab3467](https://doi.org/10.3847/1538-3881/ab3467)
- Turnbull, M. C. 2015, doi: [10.48550/ARXIV.1510.01731](https://doi.org/10.48550/ARXIV.1510.01731)
- van der Walt, S., Colbert, S. C., & Varoquaux, G. 2011, *Comput. Sci. Eng.*, 13, 22, doi: [10.1109/mcse.2011.37](https://doi.org/10.1109/mcse.2011.37)
- Virtanen, P., Gommers, R., Oliphant, T. E., et al. 2020, *Nat. Methods*, 17, 261, doi: [10.1038/s41592-019-0686-2](https://doi.org/10.1038/s41592-019-0686-2)
- Walmsley, M., Smith, L., Lintott, C., et al. 2019, *MNRAS*, 491, 1554, doi: [10.1093/mnras/stz2816](https://doi.org/10.1093/mnras/stz2816)
- Waskom, M. 2021, *JOSS*, 6, 3021, doi: [10.21105/joss.03021](https://doi.org/10.21105/joss.03021)
- Yu, H., Yang, X., Zheng, S., & Sun, C. 2019, *IEEE Transactions on Neural Networks and Learning Systems*, 30, 1088, doi: [10.1109/tnnls.2018.2855446](https://doi.org/10.1109/tnnls.2018.2855446)
- Zeraatgari, F. Z., Hafezianzadeh, F., Zhang, Y., et al. 2023, *MNRAS*, 527, 4677, doi: [10.1093/mnras/stad3436](https://doi.org/10.1093/mnras/stad3436)
- Zhang, H., Liu, W., Shan, J., & Liu, Q. 2018, *IEEE Access*, 6, 73815, doi: [10.1109/access.2018.2882872](https://doi.org/10.1109/access.2018.2882872)
- Škoda, P., Podsztavek, O., & Tvrdík, P. 2020, *A&A*, 643, A122, doi: [10.1051/0004-6361/201936090](https://doi.org/10.1051/0004-6361/201936090)